

# Transport and retention of biochar particles in porous media: effect of pH, ionic strength, and particle size

Wei Zhang,<sup>1</sup> Jianzhi Niu,<sup>2</sup> Verónica L. Morales,<sup>1</sup> Xincui Chen,<sup>3,5</sup> Anthony G. Hay,<sup>3</sup> Johannes Lehmann<sup>4</sup> and Tammo S. Steenhuis<sup>1\*</sup>

<sup>1</sup> Department of Biological and Environmental Engineering, Cornell University, Ithaca, NY 14853, USA

<sup>2</sup> College of Soil and Water Conservation, Beijing Forestry University, Beijing 100083, China

<sup>3</sup> Department of Microbiology, Cornell University, Ithaca, NY 14853, USA

<sup>4</sup> Department of Crop and Soil Sciences, Cornell University, Ithaca, NY 14853, USA

<sup>5</sup> Department of Environmental Engineering, Zhejiang University, Hangzhou 310029, China

## ABSTRACT

Biochar land application can potentially be used for carbon sequestration, improving soil quality, and reducing non-point source pollution. Understanding biochar mobility is important because its transport in soil greatly influences its stability, the dynamics of soil microbial communities and organic matter, and the movement of biochar-associated contaminants. Here, the transport of biochar particles was studied in saturated and unsaturated sand columns by measuring breakthroughs of biochar pulse under three pH and two ionic strength (IS) levels. Breakthrough curves (BTCs) were fitted to a convection–dispersion model with kinetic and equilibrium deposition sites to estimate the key transport parameters (e.g. biochar deposition rate coefficients). Biochar retention was enhanced by lowering pH and increasing IS, corroborating the trends of fitted deposition rate coefficients. Under both saturated and unsaturated conditions, effluent mass recoveries decreased, respectively, by a factor of 6.6 or 15 when pH decreased from 10 to 4 at 10 mM IS, and by a factor of 1.4 or 3.9 when IS increased from 10 to 100 mM at pH 7. Biochar retention was greater in unsaturated media, implying that saturated flow elutes more biochar particles. The particles larger than 5.4% of median grain diameter were filtered out of suspension during passage through the media; whereas, the retention of smaller particles was clearly dependent on solution chemistry. Similar to other types of colloids, this study highlights the importance of pH, IS, particle size, and soil water saturation in controlling biochar movement by soil matrix flow. Copyright © 2010 John Wiley & Sons, Ltd.

KEY WORDS biochar; black carbon; colloid; transport; porous media; carbon sequestration

Received 11 March 2010; Accepted 7 July 2010

## INTRODUCTION

Black carbon derived from low-temperature pyrolysis of biomass (i.e. biochar, agrichar or charcoal) may in the future be produced and applied to soils in large quantities to store carbon and manage soil and water quality, and crop productivity (Lehmann *et al.*, 2006; Lehmann, 2007a,b). In addition to engineered pyrolysis, black carbon is also formed by forest fire, slash-and-burn agriculture, and incomplete combustion of fossil fuel (Mitra *et al.*, 2002; Czimczik *et al.*, 2005; Rumpel *et al.*, 2006). Hereafter black carbon, biochar, and charcoal are simply referred to as biochar (BC). A preferable approach in the pyrolysis process is to combine the production of bioenergy and BC so that one portion of biomass is converted into bioenergy (e.g. gas, bio-oil or hydrogen) and the rest made into BC. This BC can then be land-applied to soil as a carbon sink because of its recalcitrant nature (Lehmann, 2007a,b). Life cycle analyses have shown that properly implemented bioenergy and BC systems could be both carbon negative (i.e. removing

CO<sub>2</sub> from the atmosphere) and economically viable (Gaunt and Lehmann, 2008; Roberts *et al.*, 2010). In addition to sequestering carbon, land application of BC may offer other agronomic and environmental benefits through improved soil fertility, increased crop production, decreased use of chemical fertilizer, and reduced non-point source pollutions (Lehmann *et al.*, 2006, 2007b).

Once in the field BC may move laterally through soil erosion and surface runoff to surface water and vertically to deeper soil depth or groundwater (Rumpel *et al.*, 2006; Hockaday *et al.*, 2007; Guggenberger *et al.*, 2008; Major *et al.*, 2010). By analysing BC concentrations at various soil depths, its downward migration has been observed to occur at depths of 10–140 cm in several soils (Skjemstad *et al.*, 1999; Dai *et al.*, 2005; Brodowski *et al.*, 2007; Leifeld *et al.*, 2007). Major *et al.* (2010) directly measured the BC flux in dissolved and particulate forms carried by saturated flow at the field-plot scale and found that BC rapidly percolated to 30 cm in a Colombian savanna sandy Oxisol following its land application. Meanwhile, Major *et al.* (2010) also hypothesized that the largest BC flux (20–53% of applied BC) unaccounted in their mass balance was exported by surface runoff. Currently, the ecological and

\* Correspondence to: Tammo S. Steenhuis, Department of Biological and Environmental Engineering, Cornell University, 206 Riley-Robb, Ithaca, NY 14853, USA. E-mail: tss1@cornell.edu

human health implications of the BC movement remain unknown.

The transport of BC in soil is important in terms of BC stability, an important property for BC as a carbon sink, because at various soil depths microbial activity, nutrient and oxygen supply, etc. are different, thus, affecting the decomposability of BC (Lehmann *et al.*, 2006; Leifeld *et al.*, 2007). Additionally, BC actively interacts with the host soil matrix and soil microbial community, which in turn affects the stability of BC and other types of soil organic matter (Pietikäinen *et al.*, 2000; Brodowski *et al.*, 2005, 2007; Czimeczik and Massiello, 2007; Hockaday *et al.*, 2007; Wardle *et al.*, 2008; Lehmann and Sohi, 2008). The BC associated with soil mineral phase may be protected from degradation (Brodowski *et al.*, 2005; Czimeczik and Massiello, 2007), whereas porous BC particles can harbour microorganisms and increase microbial activity (Pietikäinen *et al.*, 2000). Thus, the interactions among BC, microorganisms, and soil suggest that the transport of BC is related to its stability, which is critical for employing BC land application as a carbon sequestration technique (Lehmann *et al.*, 2006, 2007b; Major *et al.*, 2010). Importantly, BC has recently been shown to sorb heavy metals and organic pollutants (Chen *et al.*, 2008; Cao *et al.*, 2009), and, thus, may serve as vehicle for facilitated transport of these compounds. Nonetheless, to date, the knowledge on the transport of BC in the landscape is still limited (Lehmann *et al.*, 2006; Major *et al.*, 2010).

Moreover, studies examining environmental factors that govern the BC transport are sparse; thus, actual mechanisms for the movement of BC have not been established (Major *et al.*, 2010). For this reason, previous discussions of past BC transport studies rarely considered soil properties including pH, ionic strength (IS), etc. Here, we focused on studying the factors influencing the transport of BC particles because they can be transported rapidly (Major *et al.*, 2010) and the colloidal BC flux is an important component of their mobility in the environment (Guggenberger *et al.*, 2008). Generally, the transport of colloids (i.e. particle smaller than 10 µm, including soil mineral fragments, organic matter, microorganisms, etc.) greatly depends on pH, IS, and particle size (McDowell-Boyer *et al.*, 1986; DeNovio *et al.*, 2004). Since in the environment soil pH ranges from extremely acid (<4.5) to highly alkaline (e.g. 10) (USDA, 1954; Sparks, 2003), soil water IS changes rapidly during rainfall infiltration, irrigation, and drainage, and the BC particles in soils have a wide size distribution (<53 µm) (Skjemstad *et al.*, 1996; Brodowski *et al.*, 2007), it is imperative to examine the effect of pH, IS, and particle size on the transport of BC particles.

Therefore, the objective of this study was to elucidate basic factors influencing the transport of BC particles, including pH, IS, and particle size, through column breakthrough experiments in saturated and unsaturated sand. Sand columns were used to remove other factors so that these specific factors can be studied. The breakthrough curves (BTCs) were fitted to a mathematical model to

estimate the key transport parameters (e.g. deposition rate coefficients) and their relationship with tested system variables. The particle retention was then explained by the Derjaguin–Landau–Verwey–Overbeek theory of colloidal interactions. Particle size in the columns' influents and effluents was characterized by microscopic methods to establish a critical ratio of particle to median grain diameter that permits the particle passage through the media.

## MATERIALS AND METHODS

### Column experiments

The BC was made from a mixture of hardwoods by fast pyrolysis at 450 °C with a retention time less than 5 s (Dynamotive, Vancouver, Canada). Selected BC properties are summarized in Table I and the analyses followed the recommended procedures of NRCS (2004) and Sims and Wolf (1995). BC powder was passed through a 75 µm sieve to obtain a size fraction (<75 µm) similar to that found in soils (Skjemstad *et al.*, 1996). The sieved particles were then used in column experiments. To obtain 500 mg l<sup>-1</sup> suspensions, sieved and air-dried BC particles (50 mg) were dispersed into 100 ml of three pH buffer solutions with pH maintained at 4 (potassium hydrogen phthalate), 7 (sodium dihydrogen phosphate:disodium hydrogen phosphate, molar ratio 1:0.6), and 10 (sodium bicarbonate:sodium carbonate, molar ratio 1:1) and IS at 10 or 100 mM. The BC addition did not change the pH of the buffer solutions. The pH buffered solutions, free of BC particles, were used as background influents in column experiments conducted in duplicates for each treatment (Table II).

Angular translucent sand with  $d_{10} = 0.27$  mm,  $d_{50} = 0.40$  mm,  $d_{90} = 0.53$  mm was used as a model porous media (Size 2, AGSCO Corporation, Hasbrouck Heights, NJ, USA), consisting of 99.5% silicon dioxide (SiO<sub>2</sub>) and trace amount of aluminium oxide, iron oxide, etc. The sand was washed with deionized (DI) water to remove dust, dried, and stored in a closed container.

Table I. Properties of the air-dried biochar (BC) used in this study.

—	Properties
Bulk density (g cm <sup>-3</sup> )	0.25–0.30
Moisture content (% by weight)	29.1 ± 4.8 <sup>a</sup>
Organic matter (% by weight)	51.0 ± 1.4
pH in water	7.2 ± 0.2
<i>Morgan extractable constituents (mg kg<sup>-1</sup>)</i>	
P	34 ± 4
K	6028 ± 672
Mg	274 ± 22
Ca	2346 ± 57
Fe	70 ± 35
Mn	48 ± 8
Zn	3.4 ± 0.7
Al	0
NO <sub>3</sub>	0
Fraction <75 µm (% by weight)	40

<sup>a</sup> The values are mean and standard deviation of five replicates.

Table II. Summary of bromide and biochar (BC) particle breakthroughs in saturated and unsaturated column experiments.<sup>a</sup>

Experiment	Measured parameters				Modelled parameters			
	$\theta$ (cm <sup>3</sup> cm <sup>-3</sup> )	$S_w$	$v$ (cm min <sup>-1</sup> )	$M_{ER}$	$D$ (cm <sup>2</sup> min <sup>-1</sup> )	$k_e$ (l kg <sup>-1</sup> )	$k_d$ (min <sup>-1</sup> )	$R^2$
Saturated	—	—	—	—	—	—	—	—
Bromide-A	0.39	1.0	0.36	1.00	0.032	—	—	0.967
Bromide-B	0.39	1.0	0.35	0.948	0.027	—	—	0.985
pH4IS10-A	0.38	1.0	0.39	0.049	0.087	0.034	0.125	0.995
pH4IS10-B	0.39	1.0	0.35	0.039	0.066	0.010	0.119	0.994
pH7IS10-A	0.39	1.0	0.36	0.136	0.048	0.017	0.065	0.998
pH7IS10-B	0.39	1.0	0.35	0.137	0.029	0.016	0.064	0.998
pH7IS100-A	0.39	1.0	0.35	0.100	0.048	0.010	0.085	0.995
pH7IS100-B	0.39	1.0	0.35	0.103	0.080	0.032	0.084	0.992
pH10IS10-A	0.39	1.0	0.38	0.296	0.082	0.025	0.049	0.994
pH10IS10-B	0.37	0.94	0.38	0.283	0.083	-0.012	0.048	0.998
Unsaturated	—	—	—	—	—	—	—	—
Bromide-A	0.22	0.56	0.34	1.04	0.074	—	—	0.992
Bromide-B	0.22	0.54	0.35	1.01	0.085	—	—	0.995
pH4IS10-A	0.23	0.57	0.33	0.010	0.096	0.024	0.166	0.927
pH4IS10-B	0.21	0.51	0.36	0.014	0.171	0.000	0.175	0.899
pH7IS10-A	0.21	0.53	0.35	0.099	0.154	0.035	0.088	0.942
pH7IS10-B	0.21	0.53	0.35	0.098	0.108	0.078	0.085	0.981
pH7IS100-A	0.17	0.44	0.44	0.021	0.616	0.095	0.226	0.945
pH7IS100-B	0.22	0.56	0.34	0.029	0.097	-0.012	0.129	0.945
pH10IS10-A	0.24	0.59	0.32	0.172	0.101	0.002	0.057	0.993
pH10IS10-B	0.21	0.53	0.36	0.188	0.173	0.010	0.061	0.999

<sup>a</sup>  $\theta$  = average volumetric water content;  $S_w$  = average degree of water saturation;  $v$  = average pore water velocity;  $M_{ER}$  = mass recovery in effluents;  $D$  = hydrodynamic dispersion coefficient;  $k_e$  = partition coefficient at linear equilibrium deposition site;  $k_d$  = the first-order particle deposition rate coefficient.

A transparent acrylic column of 10-cm-long (L) and 2 × 2-cm-wide was wet-packed with the sand to a porosity ( $\theta_0$ ) of 0.39–0.40 cm<sup>3</sup> cm<sup>-3</sup>. The experimental procedure has been previously used in studying polystyrene colloids (Morales *et al.*, 2009; Zhang *et al.*, 2010). Briefly, the column experiments were conducted at a steady-state inflow and outflow rate ( $q$ ) of 0.3 ml min<sup>-1</sup> (i.e. Darcy velocity  $U = 0.075$  cm min<sup>-1</sup>) for unsaturated experiments and 0.56 ml min<sup>-1</sup> ( $U = 0.14$  cm min<sup>-1</sup>) for saturated experiments, controlled by a dual-channel peristaltic pump (MasterFlex<sup>®</sup> C/L, Cole-Parmer, Vernon Hills, IL, USA). Prior to injection of a 9 ml BC pulse input ( $C_0 = 500$  mg l<sup>-1</sup>), the columns were flushed with the BC-free background influents to stabilize the background effluent absorbance. Immediately before the pulse injection the input BC suspension was briefly sonicated for 5 min to disperse the particles. During the injection of the BC input pulse, the BC suspension was stirred periodically to prevent the particles from settling. After the injection of the BC pulse, the inflow was immediately switched back to the BC-free background influent until the effluent absorbance returned to the background absorbance level. Effluent samples were collected at either 5- or 3-min intervals for the unsaturated and saturated experiments, respectively. In separate column experiments, a pulse of bromide solution in DI water (100 mg l<sup>-1</sup>) was applied instead of the BC to define the water flow in the columns. At the end of the column experiments, the volumetric moisture content ( $\theta$ ) was measured by determining water mass in the

columns and using water density of 1.0 g cm<sup>-3</sup>. BC particle concentration was measured by a spectrophotometer at the wavelength of 550 nm (SPECTRONIC 501, Milton Roy, Ivyland, PA, USA) and the calibration curves had a linearity range of 0–500 mg l<sup>-1</sup> ( $R^2 = 0.9997$ ). The particle concentration ( $C$ ) was determined from sample absorbance after subtracting the background effluent value. The bromide concentrations were measured via ion chromatography (IC) (Dionex ICS-2000 with Ion Pac<sup>®</sup> AS18 column, Dionex, Sunnyvale, CA, USA). The normalized effluent concentrations ( $C/C_0$ ) are plotted against the number of pore volume to obtain the BTCs. The pore volume in unsaturated experiments is the product of the saturated pore volume and the degree of water saturation ( $S_w = \theta/\theta_0$ ). The experimental parameters, including experimental treatments,  $\theta$ ,  $S_w$ , and pore water velocity ( $v = U/\theta$ ), are listed in Table II.

### Modelling

The transport of particles (e.g. colloids) through porous media at a steady state flow rate is governed by the convection–dispersion equation with terms accounting for particle deposition and release (Kretzschmar *et al.*, 1997; Smith *et al.*, 2008; Morales *et al.*, 2009). Here, the deposition terms lumps all particle-retention processes in saturated and unsaturated porous media, including attachment, mechanical filtration, and straining (McDowell-Boyer *et al.*, 1986; DeNovio *et al.*, 2004; Bradford *et al.*, 2006). Attachment involves the collision of particles with

and subsequent retention at the grain surface through diffusion, interception, and sedimentation; thus, colloidal interactions and hydrodynamics are among the main determinants. Mechanical filtration occurs at the soil surface when particles or aggregates are larger than all of the soil pores, whereas straining refers to particle retention at the intersection of multiple interfaces in the soil pore, i.e. the grain–grain contacts, water film, and the air–water–solid (AWS) interfaces, thus, controlled by both physical and chemical factors (Bradford *et al.*, 2007).

For both saturated and unsaturated media we assumed that there are two types of particle deposition sites, including a kinetic irreversible deposition site and a linear reversible equilibrium deposition site (Morales *et al.*, 2009). This model is from here on referred to as the kinetic and equilibrium deposition model (KEDM). The governing equation is

$$\frac{\partial C}{\partial t} = D \frac{\partial^2 C}{\partial z^2} - v \frac{\partial C}{\partial z} - \frac{\rho_b}{\theta} \left( \frac{\partial S_1}{\partial t} + \frac{\partial S_2}{\partial t} \right) \quad (1)$$

where  $C$  ( $\text{mg l}^{-1}$ ) is the particle concentration in the liquid phase,  $t$  (min) is the elapsed time,  $D$  ( $\text{cm}^2 \text{min}^{-1}$ ) is the longitudinal hydrodynamic dispersion coefficient,  $z$  (cm) is the travel distance,  $v$  ( $\text{cm min}^{-1}$ ) is the pore water velocity,  $\rho_b$  ( $\text{g cm}^{-3}$ ) is the bulk density of packed media,  $\theta$  ( $\text{cm}^3 \text{cm}^{-3}$ ) is the moisture content in the media (i.e. the porosity  $[\theta_0]$  under saturated conditions), and  $S_1$  ( $\text{mg kg}^{-1}$ ) and  $S_2$  ( $\text{mg kg}^{-1}$ ) are the deposited particle concentrations in the solid phase by the two deposition sites. The particle deposition at the equilibrium site follows a linear isotherm

$$S_1 = k_e C \quad (2)$$

where  $k_e$  ( $\text{l kg}^{-1}$ ) is the equilibrium partition coefficient. Thus, the particle deposition rate is determined as

$$\frac{\partial S_1}{\partial t} = k_e \frac{\partial C}{\partial t} \quad (3)$$

We further assumed a first-order deposition rate coefficient ( $k_d$ ) for the kinetic site. Then, the kinetic deposition rate becomes

$$\frac{\partial S_2}{\partial t} = \frac{\theta}{\rho_b} k_d C \quad (4)$$

We also tested two other particle transport models that include a release term (Smith *et al.*, 2008) or exclusively the kinetic deposition term (Kretzschmar *et al.*, 1997; Chen *et al.*, 2007). Their governing equations and comparison with the KEDM are presented in Appendix A (Figure A1). The KEDM gave the best fit; thus, it was used. The fitting of the KEDM was implemented in CXTFIT 2.1 (Toride *et al.*, 1995) using the third-type boundary condition and a pulse input. For the bromide, all the retention terms in the models were equal to 0 (i.e.  $k_e$  and  $k_d = 0$ ) and the governing equation was reduced to the convection–dispersion equation. During the fitting of the BC BTCs to the KEDM, the parameters  $D$ ,  $k_d$ , and  $k_e$  were estimated.

### Particle size measurement

A digital bright field microscope (BFM) (KH-7700, Hirox-USA, River Edge, NJ, USA) with a resolution of  $0.278 \mu\text{m}/\text{pixel}$  was used to measure particle size in the influent and effluent from the saturated experiments (pH7IS10 and pH10IS10), since these experiments eluted more BC particles, as shown in the result section. Briefly, a liquid sample of  $10 \mu\text{l}$  was placed on a glass slide and then covered with a cover slide. Microscopic images were taken randomly at the 25 locations per sample. A total 50 images were taken for the influent samples and 25 images were taken for the effluent samples. Images were analysed for particle size using a marco routine developed in ImageJ 1.41o (Wayne Rasband, National Institutes of Health, USA). The image was first converted to an 8-bit image, the background subtracted using a rolling radius of 150 pixels, the brightness and contrast adjusted, and finally the threshold was adjusted. The particle analyses on the adjusted images allowed counting of the number of identified particles and measurement of other parameters, including particle area ( $A_p$ ), particle perimeter ( $P$ ), Feret's diameter ( $d_F$ , the longest distance between any two points along the selected particle boundary), major axis of the best fitting ellipse over particle ( $X_1$ ), minor axis of the fitting ellipse ( $X_2$ ), and aspect ratio ( $\text{AR} = X_1/X_2$ ). The particle size distribution was constructed against  $d_F$ , based on either the number of particles or the total area of particles in a particle size fraction. Here, the particle area was considered as a surrogate for its mass (Zevi *et al.*, 2006, 2009), which allowed the approximate construction of the particle size distribution by mass. This construction using particle area only gave a coarse approximation because of the lacking of the third dimension in the measurement.

To examine the lower limit of particle size, the influent and effluent particles in the saturated experiment of pH10IS10 were imaged by transmission electron microscopy (TEM) (FEI Tecnai T-12 TWIN, Hillsboro, OR, USA). The smallest particle size was measured in ImageJ, and the existence of these small particles in the bulk solution were confirmed by dynamic light scattering (Zetasizer Nano-ZS, Malvern Instruments Ltd., Malvern, Worcestershire, UK) after filtering through  $0.1 \mu\text{m}$  mixed cellulose membrane (Millipore, Burlington, MA, USA). Dynamic light scattering was not a suitable method for measuring the BC size distribution because the BC suspension was highly polydispersed. However, the technique can be used to confirm the existence of submicron particles after filtering out the particles larger than  $0.1 \mu\text{m}$ .

### DLVO interactions

In addition to the mechanical filtration of large particles, the breakthrough of BC particles is also expected to depend on colloidal interactions between BC colloids and various interfaces in the soil pores, including the solid–water interface (SWI), the air–water interface (AWI), and the air–water–solid (AWS) interfaces (DeN-ovio *et al.*, 2004; Bradford *et al.*, 2008; Zevi *et al.*, 2009).

Thus, we calculated the DLVO energy ( $\Phi$ ) as the sum of Lifshitz–van der Waals ( $\Phi^{LVW}$ ), electric double layer ( $\Phi^{EDL}$ ), and Born repulsion ( $\Phi^{BNR}$ ) interactions for a BC colloid interacting with SWI, AWI or another BC colloid (Zhang *et al.*, 2010). The negative DLVO energy at primary energy minimum or secondary energy minimum indicates an attractive force that contributes to colloid aggregation or attachment, whereas the positive  $\Phi$  suggests a repulsive force that promotes colloid stability or mobility. To calculate the DLVO energy, the  $\zeta$ -potentials of the sand surface and the BC colloids were determined. Quartz fragments were liberated from the sand by sonication in DI water for 30 min (Zevi *et al.*, 2009; Zhang *et al.*, 2010). The quartz suspension was filtered through 0.45  $\mu\text{m}$  filter membrane and the filtrates diluted into the select pH buffered solutions for electrophoretic mobility (EM) measurements by the Zetasizer. Similarly, the BC fragments were liberated from the BC suspensions in the pH buffered solutions, and the filtrates were used in the EM measurements. The  $\zeta$ -potentials of the sand surface and BC particle were calculated from the EM values using the Smoluchowski equation and listed in Table III.

A much idealized DLVO approach was used by assuming BC colloids as smooth spheres because the equations for rough and irregular surfaces are currently not available. In addition, BC particle of 1  $\mu\text{m}$  in diameter was selected to calculate the DLVO energies. Although the approach was idealized, the energy calculations still captured the qualitative trends with pH and IS. The primary energy minimum ( $\Phi_{1\text{min}}$ ), the primary energy barrier ( $\Phi_{\text{max}}$ ), and the secondary energy minimum ( $\Phi_{2\text{min}}$ ) were identified in the DLVO energy profiles. The detailed equations for DLVO energy are presented in Appendix B.

## RESULTS

### Column experiments and modelling

As shown in Table II, the particle effluent mass recoveries decreased with lowering pH and increasing IS. For example, under both saturated and unsaturated conditions the effluent mass recoveries decreased respectively by a factor of 6.6 or 15 when pH decreased from 10 to 4 at IS = 10 mM, and by a factor of 1.4 or 3.9 when IS increased from 10 to 100 mM at pH 7. The percentage of particles eluted in saturated experiments was greater than unsaturated experiments by 38–302% under otherwise same experimental conditions (Table II).

For the conservative bromide tracer, the convection–dispersion equation fitted its BTCs well ( $R^2 > 0.967$ , Table II; Figure 1). For the BC particle transport, the KEDM fitted the BTCs very well ( $R^2 > 0.992$ ) in saturated experiments, and satisfactorily ( $R^2 > 0.899$ ) in unsaturated experiments. The lower  $R^2$  values for the experiment pH4IS10 and pH7IS100 in unsaturated media could be a result of the fact that the effluent particle concentrations were too low to form well-shaped BTCs. The estimated deposition rate coefficients ( $k_d$ ) increased by lowering pH and increasing IS (Figure 2). For instance, in both saturated and unsaturated media  $k_d$  increased at least by a factor of 2.5 when pH decreased from 10 to 4, and by a factor of 1.7 to 3.0 when IS changed from 10 to 100 mM (Table II). The deposition rate coefficients were greater under unsaturated conditions than under saturated conditions (Figure 2).

### Colloidal interactions

The DLVO energies of BC colloid interacting with the sand surface (SWI) and another colloid under select experimental conditions are summarized in Table IV. The energy profiles including the colloid–AWI interaction profile are presented in Appendix B (Figure B1). For colloid–SWI interactions, the primary energy minimum ( $\Phi_{1\text{min}}$ ) existed at pH4IS10 and pH7IS100, but not at pH7IS10 and pH10IS100. The heights of the primary energy barrier ( $\Phi_{\text{max}}$ ) increased with pH at IS = 10 mM, but decreased with IS at pH 7. The depth of the secondary energy minimum ( $\Phi_{2\text{min}}$ ) was also greater at the lower pH and higher IS. For colloid–colloid interactions,  $\Phi_{1\text{min}}$  existed for pH4IS10 and pH7IS100, and there was no  $\Phi_{\text{max}}$  and  $\Phi_{2\text{min}}$  because the remainder of the energy profile was negative (Figure B1). For pH7IS10 and pH10IS10, there was no  $\Phi_{1\text{min}}$ , whereas  $\Phi_{\text{max}}$  was very high and  $\Phi_{2\text{min}}$  was shallow (Table IV). These energy profiles suggested that BC colloid aggregation and attachment to the sand would be highly favourable under pH4IS10 and pH7IS100 conditions, and much less favourable at pH7IS10 and pH10IS10.

### Particle size measurement

Representative BFM and TEM images of the BC particles in the influents and effluents are shown in Figure 3. The particle analyses showed that BC particles had very irregular shapes and a wide size distribution (Table V, Figures 3 and 4). Although the particles smaller than

Table III. Properties of background influents and electrophoretic mobility (EM) and  $\zeta$ -potentials of quartz sand and biochar (BC) colloids.

pH	IS (mM)	Quartz sand		Biochar	
		EM ( $\mu\text{m cm s}^{-1} \text{V}^{-1}$ )	$\zeta$ (mV)	EM ( $\mu\text{m cm s}^{-1} \text{V}^{-1}$ )	$\zeta$ (mV)
4.2 $\pm$ 0.2	10	−2.86 $\pm$ 0.10	−36.4 $\pm$ 1.3	−0.72 $\pm$ 0.20	−9.2 $\pm$ 2.6
6.8 $\pm$ 0.1	10	−3.62 $\pm$ 0.22	−46.1 $\pm$ 2.8	−3.04 $\pm$ 0.18	−38.7 $\pm$ 2.4
6.7 $\pm$ 0.1	100	−2.47 $\pm$ 0.28	−31.5 $\pm$ 3.5	−1.57 $\pm$ 0.16	−20.0 $\pm$ 2.0
10.0 $\pm$ 0.1	10	−3.86 $\pm$ 0.11	−49.3 $\pm$ 1.4	−4.80 $\pm$ 0.13	−61.2 $\pm$ 1.7

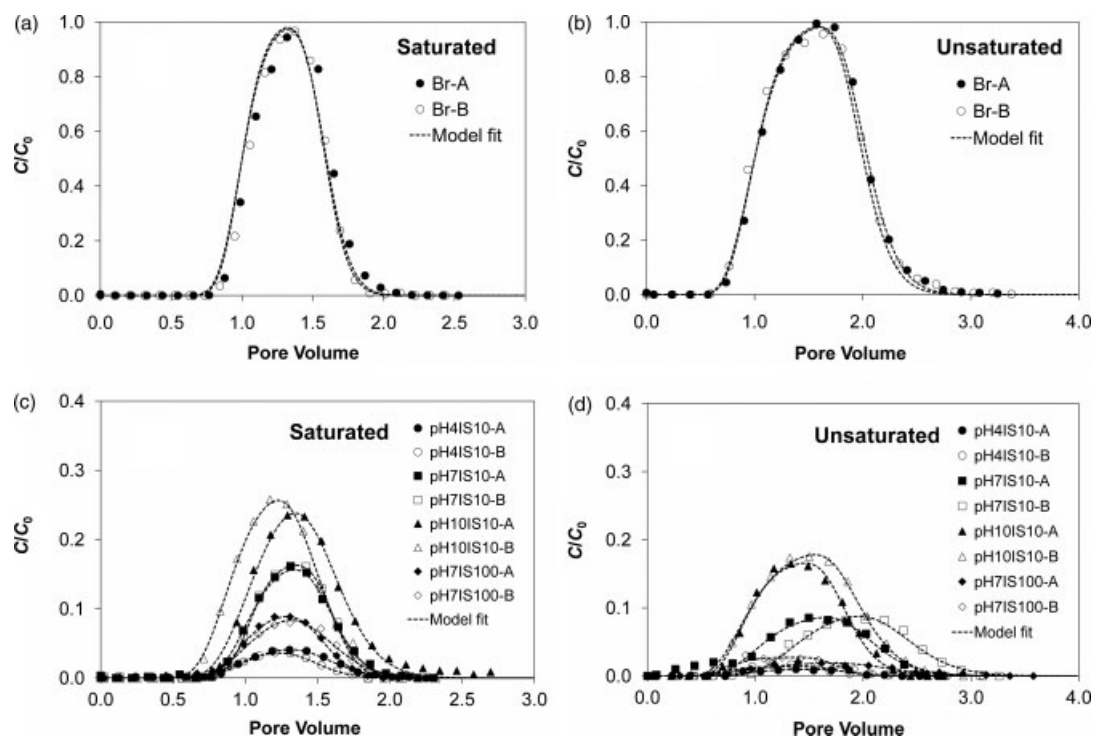


Figure 1. Measured and fitted breakthrough curves (BTCs) for bromide and biochar (BC): (a) bromide in saturated media; (b) bromide in unsaturated media; (c) BC in saturated media; and (d) BC in unsaturated media.

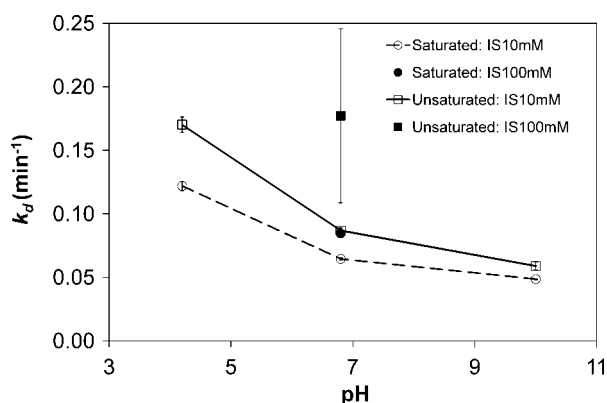


Figure 2. Deposition rate coefficients ( $k_d$ ) as function of pH and ionic strength (IS) in saturated and unsaturated media. Error bar = standard deviation of two tests.

10  $\mu\text{m}$  were dominant in number in both influents and effluents, their percentage by mass was small in the influents and became more significant in the effluents (Figure 4). The largest effluent Feret's diameter ( $d_F$ ), major axis ( $X_1$ ), and minor axis ( $X_2$ ) were 21.4, 19.8, and 8.5  $\mu\text{m}$  in the effluents (Table V). Other larger particles present in the influent were filtered out of suspension during passage through the media (Figure 4). The smallest measured BC particles were  $2.4 \pm 0.5$  nm in the influent and  $2.2 \pm 0.6$  nm in the effluent, as estimated from TEM images (Figure 3). The existence of these BC nanoparticles in the bulk solution was confirmed by dynamic light scattering, measuring the particles of  $1.4 \pm 0.6$  nm and  $1.3 \pm 0.5$  nm in the influent and effluents. Because the irregular shape of BC particles, in order to obtain a representative estimation for the ratio of the largest effluent

particle to mean grain diameter it was determined based on  $d_F$ ,  $X_1$ , and  $X_2$ , which was 0.054 ( $d_F/d_{50}$ ), 0.050 ( $X_1/d_{50}$ ), and 0.021 ( $X_2/d_{50}$ ). Since  $d_F/d_{50}$  is the upper limit of the ratio, it can be said that particles with the size smaller than 5.4% of the median grain diameter may pass through the media, while other larger particles will be removed by mechanical filtration or straining.

## DISCUSSION

### BC particle transport and retention

The transport and retention of BC particles were strongly dependent on pH and IS, which agreed with the studies on other types of colloids (DeNovio *et al.*, 2004; Bradford *et al.*, 2008; Zevi *et al.*, 2009). At the lower solution pH, the BC particles were less negatively charged (Table III), thus, reducing electrostatic repulsion, whereas greater IS decreased the electric double layer thickness and weakened the electrostatic repulsion (Figure B1). Compared with the newly prepared BC used in this study, the field BC will acquire more negative surface charge over time through abiotic and biotic oxidation with increased oxygen-containing functional groups (e.g. carboxylic and phenolic groups) (Cheng *et al.*, 2006, 2008), which may result in increased BC mobility and more pronounced dependence of the BC transport on pH and IS because of elevated charge density and electrostatic repulsion.

The BC particles had a wide size distribution from a few tens of microns to a few nanometers, similar to the BC particles observed in the field (Skjemstad *et al.*, 1996; Lehmann *et al.*, 2007b). Thus, while the mechanisms of mechanical filtration, attachment, and straining (Bradford

Table IV. Total Derjaguin–Landau–Verwey–Overbeek (DLVO) interaction energy parameters for 1  $\mu\text{m}$  biochar (BC) colloid interacting with another colloid or the solid-water interface (SWI) as function of pH and ionic strength (IS).<sup>a</sup>

pH	IS (mM)	Colloid–SWI Interaction			Colloid–colloid Interaction		
		$\Phi_{1\text{min}}$ ( $kT$ )	$\Phi_{\text{max}}$ ( $kT$ )	$\Phi_{2\text{min}}$ ( $kT$ )	$\Phi_{1\text{min}}$ ( $kT$ )	$\Phi_{\text{max}}$ ( $kT$ )	$\Phi_{2\text{min}}$ ( $kT$ )
$4.2 \pm 0.2$	10	–661	29.2	–8.2	–108	n/a (<0) <sup>c</sup>	n/a (<0)
$6.8 \pm 0.1$	10	n/a (>0) <sup>b</sup>	879	–5.8	n/a (>0)	$1.4 \times 10^9$	–8.7
$6.7 \pm 0.1$	100	–195	23.7	–33.4	–91.1	n/a (<0)	n/a (<0)
$10.0 \pm 0.1$	10	n/a (>0)	1650	–5.3	n/a (>0)	$1.4 \times 10^9$	–7.2

<sup>a</sup>  $\Phi_{1\text{min}}$  = the depth of the primary energy minimum;  $\Phi_{\text{max}}$  = the height of the primary energy barrier;  $\Phi_{2\text{min}}$  = the depth of the secondary energy minimum;  $k$  = Boltzmann constant; and  $T$  = temperature in Kelvin.

<sup>b</sup> n/a (>0) means that the negative energy minimum is not available.

<sup>c</sup> n/a (<0) means that the energy profile is always negative after the primary energy minimum.

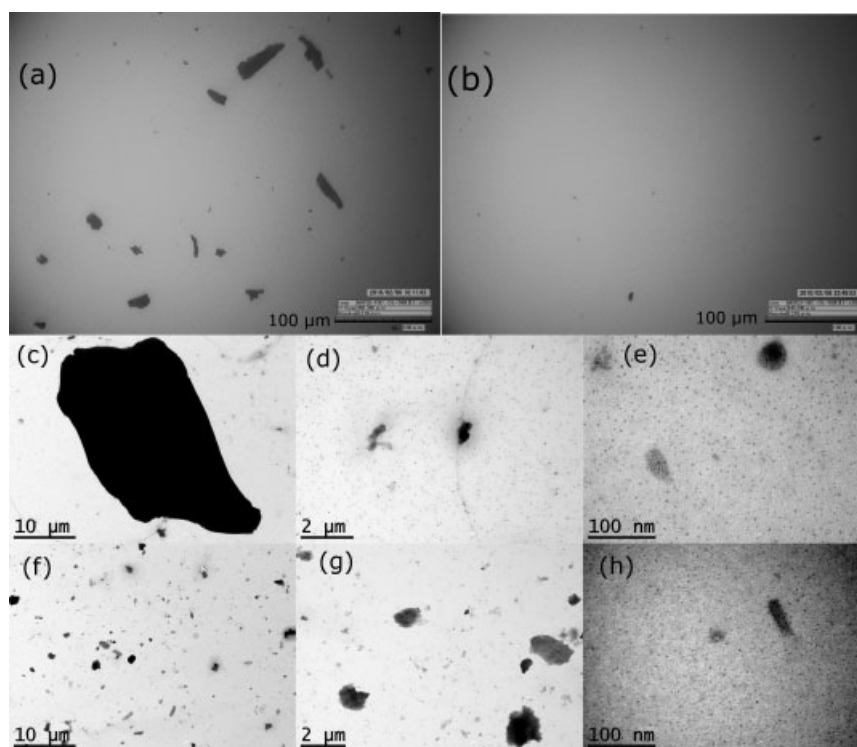


Figure 3. Microscopic images of biochar (BC) particles in the column influent and effluent under pH 10 and IS = 10 mM, taken by bright field microscopy (a and b) and transmission electron microscopy (c–h): (a) BC in the influent; (b) BC in the effluent; (c–e) BC in the influent; (f–h) BC in the effluent.

*et al.*, 2006) all likely contribute to the BC retention, the transport of smaller particles was most possibly affected by colloidal interactions that led to the attachment or aggregation. It was not possible to discern the exact contribution of each retention mechanism to the retention of each particle size class because accurate measurement of the effluent particle mass based on the size class is extremely difficult, considering the wide size distribution and irregular particle shapes. Nonetheless, in principle, it was expected that the larger particles ( $d_F > 21.4 \mu\text{m}$ ) were to a greater extent retained by mechanical filtration, whereas the transport of the smaller ones ( $d_F < 21.4 \mu\text{m}$ ) was clearly dependent on attachment, as influenced by solution chemistry. For straining to occur in uniform sand it has been estimated from geometric relations that the ratio of particle to median grain diameter needs to be greater than 0.18; however, ratios as low as 0.003 have

also been previously observed (Bradford *et al.*, 2006). Here the ratio of the largest effluent particle to median grain diameter ranged from 0.021 to 0.054, indicating that straining could be an important process for the BC retention. Additionally, straining is coupled with colloidal interactions (e.g. small soil pores, wedge-shaped pore spaces, etc.) in that straining sites are optimum locations for colloid attachment due to reduced flow drag force, and colloidal interactions enhance straining (Bradford *et al.*, 2006, 2007). More evidence supporting the effect of solution chemistry on the BC retention is shown in the trends of deposition rate coefficients with pH and IS (Figure 2). These trends qualitatively agreed with DLVO interaction energy profiles.

As expected, the BC particle retention was significantly greater in unsaturated experiments than in saturated experiments (Bradford *et al.*, 2006; Chen *et al.*, 2007).

Table V. Summary of biochar (BC) particle size in the influent and effluent.<sup>a</sup>

Conditions	$A_p$ ( $\mu\text{m}^2$ )	$P$ ( $\mu\text{m}$ )	$d_F$ ( $\mu\text{m}$ )	$X_1$ ( $\mu\text{m}$ )	$X_2$ ( $\mu\text{m}$ )	AR
<i>pH7IS10</i>						
Influent						
Maximum	4300	615	159	151	43.9	10.0
Minimum	0.2	1.2	0.6	0.6	0.3	1.0
Mean (standard deviation)	22.7 (155)	10.1 (30.6)	3.4 (8.5)	3.0 (7.7)	1.5 (3.4)	2.0 (0.8)
Effluent						
Maximum	123	67.3	20.3	18.3	8.5	5.2
Minimum	0.1	1.1	0.5	0.4	0.2	1.0
Mean (standard deviation)	2.0 (9.9)	4.5 (6.6)	1.7 (2.0)	1.5 (1.8)	0.8 (0.8)	2.0 (0.7)
<i>pH10IS10</i>						
Influent						
Maximum	2500	489	109	110	40.8	11.8
Minimum	0.2	1.2	0.6	0.6	0.3	1.0
Mean (standard deviation)	18.9 (110)	10.3 (29.2)	3.4 (8.1)	3.1 (7.4)	1.5 (3.1)	2.0 (0.8)
Effluent						
Maximum	86.9	56.8	21.4	19.8	6.4	7.9
Minimum	0.2	1.2	0.6	0.6	0.3	1.0
Mean (standard deviation)	3.1 (7.5)	6.4 (7.3)	2.5 (2.5)	2.2 (2.2)	1.0 (0.9)	2.2 (1.0)

<sup>a</sup>  $A_p$  is the two dimensional area of particle;  $P$  = the perimeter of particle;  $d_F$  = Feret's diameter;  $X_1$  = the major axis;  $X_2$  = the minor axis; AR = the aspect ratio ( $X_1/X_2$ ).

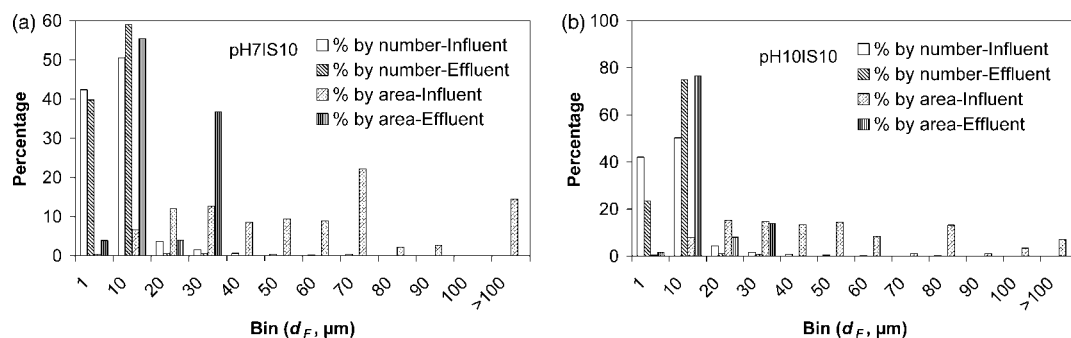


Figure 4. Particle size distribution in the column influents and effluents: (a) pH 7 and IS = 10 mM; (b) pH 10 and IS = 10 mM.

This effect is likely a result of the flow restricted to smaller soil pore spaces, water film around sand grain, and the expansion of AWS interfaces at lower moisture content; thus, resulting in greater deposition rates (Bradford *et al.*, 2006; Chen *et al.*, 2007; Zhang *et al.*, 2010). Although it is difficult to assess the degree to which this enhancement of retention will affect particles of various sizes, it is anticipated that it will preferentially increase the retention of larger particles because the water flow is restricted to smaller soil pore spaces, which allows the retention of larger particles but the passage of smaller ones (Bradford *et al.*, 2006).

For the tested BC, the size fraction ( $<75 \mu\text{m}$ ) used in this study accounted for approximately 40% (by weight) of the total BC powder. The greatest effluent recoveries occurred in the saturated experiments of pH10IS10 and about 29% of the input mass (approximately 12% of the total original mass) was eluted. The transport of BC was lowest at pH 4 (less than 2% of the total mass). Although our result is directly applicable to coarse sandy soils or sediments, the fraction transported in finer textured soils would likely be different.

### Implications

The results of this study suggest that the BC transport by soil matrix flow in the field is expected to greatly depend on soil water chemistry (i.e. pH and IS) and particle size. Attachment or sorption of BC to soil minerals equally depends on soil pH, as the positive charge of variable-charge iron or alumina oxides may significantly decrease at high pH (e.g. 9.7) (Kosmulski, 2001) and may partially explain the observed difference in leaching at different soil pH. Guggenberger *et al.* (2008) observed that the lowest BC concentrations in the stream occurred during the summer low flow period when stream pH was 9.7. These authors implied that it could have been due to the sorption of BC to the mineral soil, but did not explicitly consider soil pH. Thus, there is an evident need to consider the chemistry of soil and soil water when interpreting the mobility and transport of BC in the field. The BC particle size also played a role, as particles larger than 5.4% of median grain diameter were not eluted. However, only a few studies considered the particle size when studying the BC mobility. Skjemstad *et al.* (1999) suggested that the BC accumulation in deeper soil depth might be because of its fine particle size. Brodowski *et al.*

(2007) conjectured that the BC movement down the soil profile may be due to leaching of smaller BC particles. Nonetheless, the ratio of particle to median grain diameter needs to be considered in combination with soil water chemistry because of the complex interplay of physical and chemical mechanisms in colloid retention (Bradford *et al.*, 2006, 2007).

Additionally, the transport of BC particles decreased by lowering water content, thus, suggesting that the saturated flow transported more BC particles than the unsaturated flow. Also, in the artificially drained agricultural field the subsurface transport of particles may be facilitated by tile drains (Laubel *et al.*, 1999; Schelde *et al.*, 2006). Although the soil moisture content in most agricultural soils is usually at field capacity or less, saturated conditions often occur in undulating landscapes containing glaciated soils with relatively permeable shallow top soil underlain by a dense slowly permeable fragipan (e.g. the northeastern United States of America). The areas prone to saturation are known as variable source areas (VSAs) because the extent of saturation varies with rainfall and other factors (Walter *et al.*, 2000). In New York City watershed, Walter *et al.* (2000) estimated that VSAs could be 10% of the total watershed area and generate 20% of the total annual runoff. Thus, when the BC is applied in the VSAs of agricultural field, both surface overland flow and saturated subsurface flow (facilitated by tile drainage) may export a significant amount of BC if the areas are close to field ditch or natural waterways.

Although this study was conducted in a model system within a short term, its results could be relevant to field-scale phenomena. BC mobilization and transport in the field most likely occur during a rainfall or irrigation event that takes place in a short time (Laubel *et al.*, 1999; DeNovio *et al.*, 2004; Schelde *et al.*, 2006). Thus, this study helps understand the effect of soil water chemistry on the BC mobility, in addition to the water flux. Additionally, the BC transport in the field would be facilitated by a number of other factors, including macropore or preferential flow (McDowell-Boyer *et al.*, 1986; Laubel *et al.*, 1999; Major *et al.*, 2010), bioturbation (Carcaillet *et al.*, 2001; Brodowski *et al.*, 2007) or tillage (Skjemstad *et al.*, 1999), which warrant further studies.

### CONCLUSIONS

The findings of this study suggest that soil properties (e.g. soil pH, total salt concentrations) need to be considered for assessing the BC mobility in the field, because BC particle retention increased with lowering pH and increasing IS. As the ratio of particle to median grain diameter was an important factor, BC particle size and soil texture also warrant serious consideration. Additionally, because the greater amount of BC was transported under saturated conditions, compared with unsaturated conditions, local hydrology (e.g. soil water saturation) is an important driver of the BC transport. The long-term vertical transport of BC is likely a cumulative result of the BC movement due to the reoccurring

transport by water infiltration and drainage (e.g. soil matrix flow, macropore or preferential flow), and physical mixing by earth worms or tillage.

### ACKNOWLEDGEMENTS

The funding for this research was primarily provided by USDA-NRI, BARD, and NSF with additional funding from USDA Hatch and the Andrew W. Mellon Foundation. The authors like to thank Dr Yuanming Zhang at the Cornell Center for Materials Research for help on transmission electron microscopy and dynamic light scattering measurements and Dr Bin Gao at the University of Florida for sharing the KDRM Matlab code.

### REFERENCES

- Akbour RA, Douch J, Hamdani M, Schmitz P. 2002. Transport of kaolinite colloids through quartz sand: influence of humic acid, Ca<sup>2+</sup>, and trace metals. *Journal of Colloid and Interface Science* **253**: 1–8. DOI: 10.1006/jcis.2002.8523.
- Bradford SA, Šimůnek J, Bettahar M, van Genuchten MT, Yates SR. 2006. Significance of straining in colloid deposition: evidence and implications. *Water Resources Research* **42**: W12S15. DOI: 10.1029/2005WR004791.
- Bradford SA, Torkzaban S, Walker SL. 2007. Coupling of physical and chemical mechanisms of colloid straining in saturated porous media. *Water Research* **41**: 3012–3024. DOI: 10.1016/j.watres.2007.03.030.
- Bradford SA, Torkzaban S. 2008. Colloid transport and retention in unsaturated porous media: a review of interface-, collector-, and pore-scale processes and models. *Vadose Zone Journal* **7**(2): 667–681. DOI: 10.2136/vzj2007.0092.
- Brodowski S, Amelung W, Haumaier L, Abetz C, Zech W. 2005. Morphological and chemical properties of black carbon in physical soil fractions as revealed by scanning electron microscopy and energy-dispersive X-ray spectroscopy. *Geoderma* **128**: 116–129. DOI: 10.1016/j.geoderma.2004.12.019.
- Brodowski S, Amelung W, Haumaier L, Zech W. 2007. Black carbon contribution to stable humus in German arable soils. *Geoderma* **139**: 220–228. DOI: 10.1016/j.geoderma.2007.02.004.
- Cao X, Ma L, Gao B, Harris W. 2009. Dairy-manure derived biochar effectively sorbs lead and atrazine. *Environmental Science & Technology* **43**(9): 3285–3291. DOI: 10.1021/es803092k.
- Chen B, Zhou D, Zhu L. 2008. Transitional adsorption and partition of nonpolar and polar aromatic contaminants by biochars of pine needles with different pyrolytic temperatures. *Environmental Science & Technology* **42**(14): 5137–5143. DOI: 10.1021/es8002684.
- Chen G, Abichou T, Tawfiq K, Subramaniam PK. 2007. Impact of surface charge density on colloid deposition in unsaturated porous media. *Colloids and Surfaces A: Physicochemical and Engineering Aspects* **302**: 342–348. DOI: 10.1016/j.colsurfa.2007.02.063.
- Cheng C-H, Lehmann J, Thies JE, Burton SD, Engelhard MH. 2006. Oxidation of black carbon by biotic and abiotic processes. *Organic Geochemistry* **37**: 1477–1488. DOI: 10.1016/j.orggeochem.2006.06.022.
- Cheng C-H, Lehmann J, Engelhard MH. 2008. Natural oxidation of black carbon in soils: changes in molecular form and surface charge along a climosequence. *Geochimica et Cosmochimica Acta* **72**: 1598–1610. DOI: 10.1016/j.gca.2008.01.010.
- Carcaillet C. 2001. Are Holocene wood-charcoal fragments stratified in alpine and subalpine soils? Evidence from the Alps based on AMS <sup>14</sup>C dates. *The Holocene* **11**(2): 231–242. DOI: 10.1191/095968301674071040.
- Czimeczik CI, Schmidt MWI, Schulze E-D. 2005. Effects of increasing fire frequency on black carbon and organic matter in Podzols of Siberian Scots pine forests. *European Journal of Soil Science* **56**: 417–428. DOI: 10.1111/j.1365–2389.2004.00665.x.
- Czimeczik CI, Massiello CA. 2007. Controls on black carbon storage in soils. *Global Biogeochemical Cycles* **21**: GB3005. DOI: 10.1029/2006GB002798.

- Dai X, Boutton TW, Glaser B, Ansley RJ, Zech W. 2005. Black carbon in a temperate mixed-grass savanna. *Soil Biology & Biochemistry* **37**: 1879–1881. DOI: 10.1016/j.soilbio.2005.02.021.
- DeNovio NM, Saiers JE, Ryan JN. 2004. Colloid movement in unsaturated porous media: recent advances and future directions. *Vadose Zone Journal* **3**: 338–351.
- Feke DL, Prabhu ND, Mann JA Jr, Mann JA, III. 1984. A formulation of the short-range repulsion between spherical colloidal particles. *Journal of Physical Chemistry* **88**(23): 5735–5739. DOI: 10.1021/j150667a055.
- Gaunt JL, Lehmann J. 2008. Energy balance and emissions associated with biochar sequestration and pyrolysis bioenergy production. *Environmental Science & Technology* **42**(11): 4152–4158. DOI: 10.1021/es071361i.
- Guggenberger G, Rodionov A, Shibistova O, Grabe M, Kasansky OA, Fuchs H, Mikheyeva N, Zrazhevskaya G, Flessa H. 2008. Storage and mobility of black carbon in permafrost soils of the forest tundra ecotone in Northern Siberia. *Global Change Biology* **14**: 1367–1381. DOI: 10.1111/j.1365-2486.2008.01568.x.
- Hamaker HC. 1937. The London-van der Waals attraction between spherical particles. *Physica* **4**: 1058–1072. DOI: 10.1016/S0031-8914(37)80203-7.
- Hockaday WC, Grannas AM, Kim S, Hatcher PG. 2007. The transformation and mobility of charcoal in a fire-impacted watershed. *Geochimica et Cosmochimica Acta* **71**: 3432–3445. DOI: 10.1016/j.gca.2007.02.023.
- Hoek EMV, Agarwal GK. 2006. Extended DLVO interactions between spherical particles and rough surfaces. *Journal of Colloid and Interface Science* **298**: 50–58. DOI: 10.1016/j.jcis.2005.12.031.
- Hogg R, Healy TW, Fuerstenau DW. 1966. Mutual coagulation of colloidal dispersions. *Transactions of Faraday Society* **62**: 1638–1651. DOI: 10.1039/TF9666201638.
- Kosmulski M. 2001. *Chemical Properties of Material Surfaces*. Marcel Dekker: New York.
- Kretzschmar R, Barmettler K, Grolimund D, Yan Y-D, Borkovec M, Sticher H. 1997. Experimental determination of colloid deposition rates and collision efficiencies in natural porous media. *Water Resources Research* **33**(5): 1129–1137.
- Laubel A, Jacobsen OH, Kronvang BK, Grant R, Anderson HE. 1999. Subsurface drainage loss of particles and phosphorus from field plot experiments and a tile-drained catchment. *Journal of Environmental Quality* **28**: 576–584.
- Lehmann J, Gaunt J, Rondon M. 2006. Bio-char sequestration in terrestrial ecosystems—a review. *Mitigation and Adaptation Strategies for Global Change* **11**: 403–427. DOI: 10.1007/s11027-005-9006-5.
- Lehmann J. 2007a. A handful of carbon. *Nature* **447**: 143–144. DOI: 10.1038/447143a.
- Lehmann J. 2007b. Bio-energy in the black. *Frontiers in Ecology and the Environment* **5**(7): 381–387.
- Lehmann J, Sohi S. 2008. Comment on “Fire-derived charcoal causes loss of forest humus”. *Science* **321**: 1295c. DOI: 10.1126/science.1160005.
- Leifeld J, Fenner S, Müller M. 2007. Mobility of black carbon in drained peatland soils. *Biogeosciences* **4**: 425–432.
- Major J, Lehmann J, Rondon M, Goodale C. 2010. Fate of soil-applied black carbon: downward migration, leaching, and soil respiration. *Global Change Biology* **16**(4): 1366–1379. DOI: 10.1111/j.1365-2486.2009.02044.x.
- McDowell-Boyer LM, Hunt JR, Sitar N. 1986. Particle transport through porous media. *Water Resources Research* **22**(13): 1901–1921.
- Mitra S, Bianchi TS, McKee BA, Sutula M. 2002. Black carbon from the Mississippi River: quantities, sources, and potential implications for the global carbon cycle. *Environmental Science & Technology* **36**(11): 2296–2302. DOI: 10.1021/es015834b.
- Morales VL, Gao B, Steenhuis TS. 2009. Grain surface-roughness effects on colloid retention in the vadose zone. *Vadose Zone Journal* **8**(1): 11–20. DOI: 10.2136/vzj2007.0171.
- Norde W, Lyklema J. 1989. Protein adsorption and bacterial adhesion to solid-surfaces—A colloid-chemical approach. *Colloids and Surfaces* **38**: 1–13.
- NRCS. 2004. *Soil survey laboratory methods manual*. Soil survey investigations report No. 42. Burt R. (ed). National Resources Conservation Service: Washington DC.
- Pietikäinen J, Kiiikkilä O, Fritze H. 2000. Charcoal as a habitat for microbes and its effect on the microbial community of the underlying humus. *Oikos* **89**: 231–242. DOI: 10.1034/j.1600-0706.2000.890203.x.
- Roberts KG, Gloy BA, Joseph S, Scott NR, Lehmann J. 2010. Life cycle assessment of biochar systems: estimating the energetic, economic, and climate change potential. *Environmental Science & Technology* **44**(2): 827–833. DOI: 10.1021/es902266r.
- Ruckenstein E, Prieve DC. 1976. Adsorption and desorption of particles and their chromatographic separation. *AIChE Journal* **22**(2): 276–283. DOI: 10.1002/aic.690220209.
- Rumpel C, Chaplot V, Planchon O, Bernadou J, Valentin C, Mariotti A. 2006. Preferential erosion of black carbon on steep slopes with slash and burn agriculture. *Catena* **65**: 30–40. DOI: 10.1016/j.catena.2005.09.005.
- Schäfer A, Harms H, Zehnder AJB. 1998. Bacterial accumulation at the air-water interface. *Environmental Science & Technology* **32**(23): 3704–3712. DOI: 10.1021/es980191u.
- Schelde K, de Jonge LW, Kjaergaard C, Laegdsmand M, Rubæk GH. 2006. Effects of manure application and plowing on transport of colloids and phosphorus to tile drains. *Vadose Zone Journal* **5**: 445–458. DOI: 10.2136/vzj2005.0051.
- Sims JT, Wolf A. 1995. Recommended soil testing procedures for the Northeastern United States. Northeast Regional Bull. 493., Agricultural Experiment Station, University of Delaware, Newark, DE.
- Sparks DL. 2003. *Environmental Soil Chemistry*. Academic Press: San Diego, CA.
- Skjemstad JO, Clarke P, Taylor JA, Oades JM, McClure SG. 1996. The chemistry and nature of protected carbon in soil. *Australian Journal of Soil Research* **34**: 251–271. DOI: 10.1071/SR9960251.
- Skjemstad JO, Taylor JA, Janik LJ, Marvanek SP. 1999. Soil organic carbon dynamics under long-term sugarcane monoculture. *Australian Journal of Soil Research* **37**(1): 151–164. DOI: 10.1071/S98051.
- Smith J, Gao B, Funabashi H, Tran TN, Luo D, Ahner BA, Steenhuis TS, Hay AG, Walter MT. 2008. Pore-scale quantification of colloid transport in saturated porous media. *Environmental Science & Technology* **42**(2): 517–523. DOI: 10.1021/es070736x.
- Toride N, Leij FJ, van Genuchten MT. 1995. *The CXTFIT code for estimating transport parameters from laboratory or field tracer experiments*. Version 2.1. Research Report 137, US Salinity Lab., Riverside, CA.
- USDA. 1954. *Diagnosis and improvement of saline and alkali soils*. L.A. Richards (ed). *Agriculture Handbook* No. 60, U.S. Department of Agriculture: Washington DC.
- van Oss CJ. 1994. *Interfacial forces in aqueous media*. Marcel Dekker: New York, NY.
- Wardle DA, Nilsson M-C, Zackrisson O. 2008. Fire-derived charcoal causes loss of forest humus. *Science* **320**: 629. DOI: 10.1126/science.1160750.
- Walter MT, Walter MF, Brooks ES, Steenhuis TS, Boll J, Weiler KR. 2000. Hydrologically sensitive areas: variable source area hydrology implications for water quality risk assessment. *Journal of Soil and Water Conservation* **55**(3): 277–284.
- Xu R, Wu C, Xu H. 2007. Particle size and zeta potential of carbon black in liquid media. *Carbon* **45**: 2806–2809. DOI: 10.1016/j.carbon.2007.09.010.
- Zevi Y, Dathe A, Gao B, Richards BK, Steenhuis TS. 2006. Quantifying colloid retention in partially saturated porous media. *Water Resources Research* **42**: W12S03. DOI: 10.1029/2006WR004929.
- Zevi Y, Dathe A, Gao B, Zhang W, Brian BK, Steenhuis TS. 2009. Transport and retention of colloidal particles in partially saturated porous media: effect of ionic strength. *Water Resources Research* **45**: W12403. DOI: 10.1029/2008WR007322.
- Zhang W, Morales VL, Cakmak ME, Salvucci AE, Geohring LD, Hay AG, Parlange J-Y, Steenhuis TS. 2010. Colloid transport and retention in unsaturated porous media: Effect of colloid input concentration. *Environmental Science & Technology* **44**(13): 4965–4972. DOI: 10.1021/es100272f.

## APPENDIX A

Here we have presented the two other models for the particle transport and compared them with the KEDM for the BTCs of saturated experiments. The governing equation for the model with a kinetic deposition and release terms (i.e. KDRM) are

$$\frac{\partial C}{\partial t} = D \frac{\partial^2 C}{\partial z^2} - v \frac{\partial C}{\partial z} - \frac{\rho_b}{\theta} \frac{\partial S}{\partial t} \quad (\text{A.1})$$

$$\frac{\partial S}{\partial t} = \frac{\theta}{\rho_b} k_d C - k_r S \quad (\text{A.2})$$

where  $k_r$  ( $\text{min}^{-1}$ ) is the first-order release coefficient and  $S$  ( $\text{mg kg}^{-1}$ ) is the deposited particle concentration in the solid phase. For the model with only the kinetic deposition term (i.e. KDM), the governing equation becomes

$$\frac{\partial C}{\partial t} = D \frac{\partial^2 C}{\partial z^2} - v \frac{\partial C}{\partial z} - k_d C \quad (\text{A.3})$$

The KDM model was implemented in CXTFIT 2.1 and the KDRM in Matlab (The Mathworks, Natick, MA, USA). The dispersion coefficient ( $D$ ) of bromide was used when fitting the KDRM, whereas it was estimated as a fitting parameter in the KDM. We also used the  $D$  values from the KEDM when fitting the KDRM and found that the estimates of  $k_d$  were insensitive to the choice of the  $D$  values (Figure A1(a)). This insensitivity to  $D$  is simply because these experiments had a high Peclet number ( $\text{Pe} = vL/D$ ,  $43 < \text{Pe} < 121$ ). When  $\text{Pe}$  is high (e.g.  $\text{Pe} > 50$ ), the dispersion term in Equation (A.1) becomes negligible, and the  $k_d$  estimation is minimally related to  $D$  (Kretzschmar *et al.*, 1997; Akbour *et al.*, 2002). Compared with the KDM and KDRM, the KEDM gave the overall best fit ( $R^2 > 0.992$ ), although the  $k_d$  estimates from all three models (KEDM, KDM, and KDRM) differed by less than 7% (Figure A1(a)). Due to the explicit release term in the KDRM and its absence in the KDM, the experimental BTCs tails were overestimated by the KDRM and underestimated by the KDM in seven out of eight cases as exemplified in Figure A1(b). Thus, the KEDM was selected.

APPENDIX B

Here we have presented the detailed equations for the DLVO energy calculations. The total DLVO interaction energy ( $\Phi$ ) is determined as a function of separation distance ( $x$ )

$$\Phi(x) = \Phi^{\text{LVW}}(x) + \Phi^{\text{EDL}}(x) + \Phi^{\text{BNR}}(x) \quad (\text{B.1})$$

For colloid–colloid interaction, the non-retarded Lifshitz–van der Waals interaction energy [ $\Phi^{\text{LVW}}(x)$ ] can

be calculated as (Hamaker *et al.*, 1937)

$$\Phi^{\text{LVW}}(x) = -\frac{A}{12} \left\{ \frac{y}{r^2 + ry + r} + \frac{y}{r^2 + ry + r + y} + 2 \ln \left( \frac{r^2 + ry + r}{r^2 + ry + r + y} \right) \right\} \quad (\text{B.2})$$

where  $y = 1$  for the ratio of the radii of two identical spheres,  $r = x/(2a_c)$  and  $a_c$  is the sphere radius, and  $A$  is the Hamaker constant. For colloid–SWI and colloid–AWI interactions, the expression is (Norde and Lyklema, 1989)

$$\Phi^{\text{LVW}}(x) = -\frac{A}{6} \left\{ \frac{2a_c(x + a_c)}{x(x + 2a_c)} - \ln \left( \frac{x + 2a_c}{x} \right) \right\} \quad (\text{B.3})$$

We used the Hamaker constant of polystyrene to approximate the values of BC. The Hamaker constant is  $1.3 \times 10^{-20}$  J for colloid–water–colloid interaction,  $8.9 \times 10^{-21}$  J for colloid–water–sand interaction, and  $-1.6 \times 10^{-20}$  J for colloid–water–air interaction (Zevi *et al.*, 2009).

Assuming constant surface potentials,  $\Phi^{\text{EDL}}(x)$  of colloid–SWI or colloid–AWI interactions is (Hogg *et al.*, 1966; Hoek and Agarwal, 2006)

$$\Phi^{\text{EDL}}(x) = \pi \varepsilon \varepsilon_0 a_c \left\{ 2\psi_1 \psi_2 \ln \left[ \frac{1 + \exp(-\kappa x)}{1 - \exp(-\kappa x)} \right] + (\psi_1^2 + \psi_2^2) \ln [1 - \exp(-2\kappa x)] \right\} \quad (\text{B.4})$$

where  $\varepsilon$  is the dielectric constant of water ( $80.1$  at  $293.15$  K),  $\varepsilon_0$  is the vacuum permittivity ( $8.854 \times 10^{-12} \text{ C}^2 \text{ N}^{-1} \text{ m}^{-2}$ ),  $\psi_1$  and  $\psi_2$  are the surface potentials of the colloid, and the sand or AWI.  $\kappa$  is the reciprocal electric double layer thickness ( $\kappa^{-1}$ ).

$$\kappa^{-1} = \left( \frac{\varepsilon \varepsilon_0 k T}{2000 N_A I e^2} \right)^{1/2} \quad (\text{B.5})$$

where  $k$  is Boltzmann constant ( $1.381 \times 10^{-23} \text{ J K}^{-1}$ ),  $T$  is temperature in Kelvin,  $N_A$  is Avogadro constant ( $6.022 \times 10^{23}$ ),  $I$  is IS ( $\text{mol l}^{-1}$ ), and  $e$  is the elementary

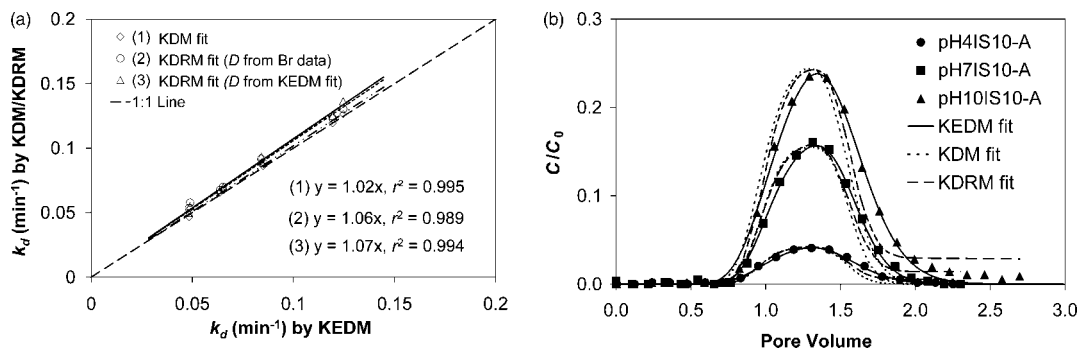


Figure A1. Comparison among the kinetic and equilibrium deposition model (KEDM), the kinetic deposition model (KDM), and the kinetic deposition and release model (KDRM) for biochar (BC) transport in saturated media: (a) comparison of deposition rate coefficient ( $k_d$ ); (b) comparison of fitted breakthrough curves (BTCs).

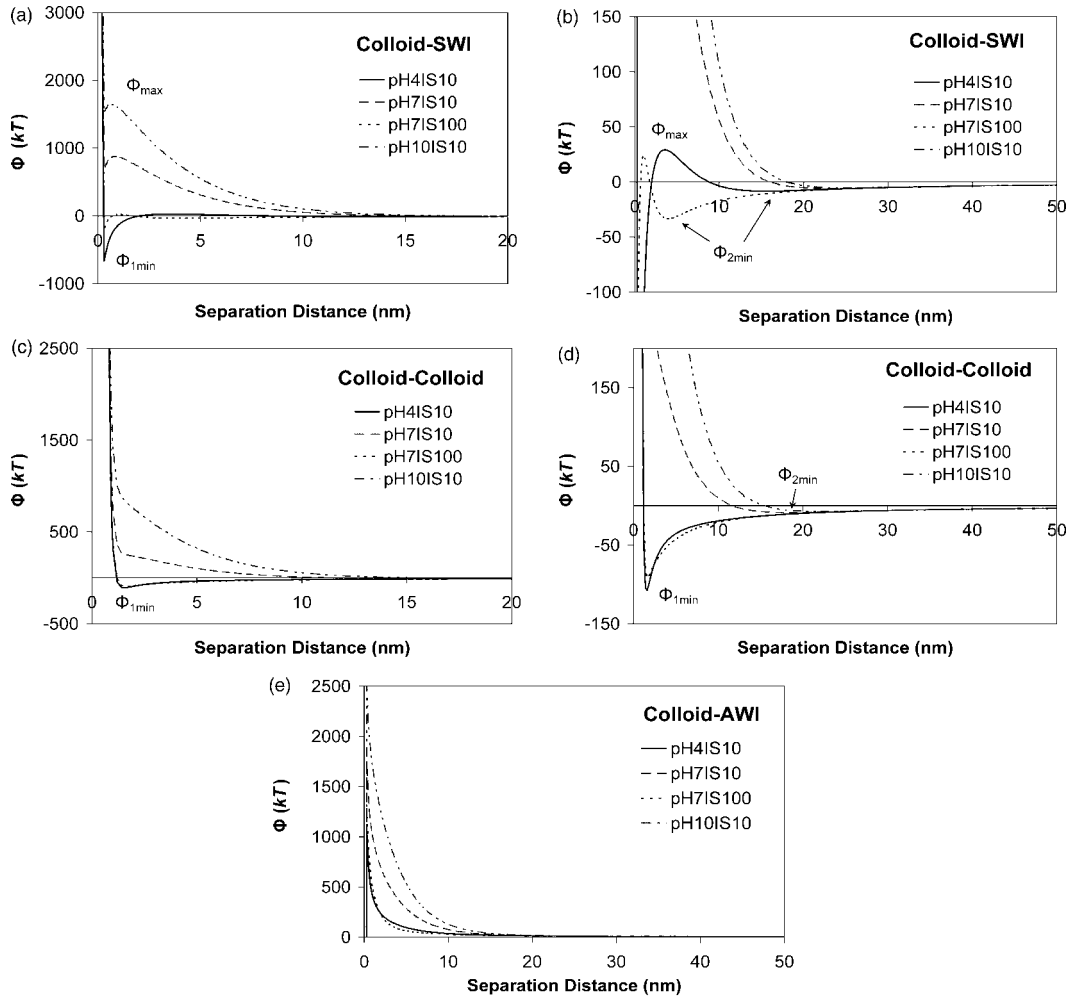


Figure B1. DLVO interaction energy ( $\Phi$ ) of a 1  $\mu\text{m}$  biochar (BC) colloid interacting with the solid-water interface (SWI), another colloid, and the air-water interface (AWI): (a) Primary energy minimum ( $\Phi_{1\text{min}}$ ) and primary energy barrier ( $\Phi_{\text{max}}$ ) of colloid–SWI interactions; (b) Secondary energy minimum ( $\Phi_{2\text{min}}$ ) of colloid–SWI interactions; (c)  $\Phi_{1\text{min}}$  and  $\Phi_{\text{max}}$  of colloid–colloid interactions; (d)  $\Phi_{2\text{min}}$  of colloid–colloid interactions; (e) colloid–AWI interactions.

charge ( $1.602 \times 10^{-19}$  C).  $\Phi^{\text{EDL}}(x)$  between two identical colloids is

$$\Phi^{\text{EDL}}(x) = \pi\epsilon\epsilon_0 a_c \left\{ \begin{array}{l} \psi_1^2 \ln \left[ \frac{1 + \exp(-\kappa x)}{1 - \exp(-\kappa x)} \right] \\ + \psi_1^2 \ln [1 - \exp(-2\kappa x)] \end{array} \right\} \quad (\text{B.6})$$

Here we used the measured  $\zeta$ -potential (Table III) in place of the surface potential (van Oss, 1994). The  $\zeta$ -potential of AWI was estimated to be  $-20$  mV at pH 4 and IS = 10 mM,  $-30$  mV at pH 7 and IS = 10 mM,  $-25$  mV at pH 7 and IS = 100 mM, and  $-40$  mV at pH 10 and IS = 10 mM (Schäfer *et al.*, 1998; Xu *et al.*, 2007).

The Born repulsion ( $\Phi^{\text{BNR}}$ ) results from the overlap of the atoms' electron clouds and is of short range.  $\Phi^{\text{BNR}}$  for colloid–SWI or colloid–AWI interactions is (Ruckenstein and Prieve, 1976)

$$\Phi^{\text{BNR}}(x) = \frac{A\sigma^6}{7560} \left[ \frac{8a_c + x}{(2a_c + x)^7} + \frac{6a_c - x}{x^7} \right] \quad (\text{B.7})$$

where  $\sigma$  is the collision diameter (0.5 nm).  $\Phi^{\text{BNR}}(x)$  for colloid–colloid interaction is (Feke *et al.*, 1984)

$$\Phi^{\text{BNR}}(x) = 4A \left( \frac{\sigma}{a_c} \right)^6 \frac{4!}{10!} \left[ \frac{(x/a_c)^2 - 14x/a_c + 54}{(x/a_c - 2)^7} + \frac{-2(x/a_c)^2 + 60}{(x/a_c)^7} + \frac{(x/a_c)^2 + 14x/a_c + 54}{(x/a_c + 2)^7} \right] \quad (\text{B.8})$$

The DLVO energy profiles for three types of colloidal interactions are presented in Figure B1. In addition to the discussion in the main text, there was a great repulsive energy barrier between colloid and the AWI. There was no secondary energy minimum  $\Phi_{2\text{min}}$  up to separation distance of 2000 nm. The negative primary energy for colloid–AWI interaction stems from its negative Hamaker constant, which resulted in the negative Born repulsion. This  $\Phi_{1\text{min}}$  is irrelevant here because the colloids could hardly pass through the high energy barrier to reach this minimum.